ACS SENSORS

pubs.acs.org/acssensors

Article

iGIST—A Kinetic Bioassay for Pertussis Toxin Based on Its Effect on Inhibitory GPCR Signaling

Valeriy M. Paramonov, Cecilia Sahlgren, Adolfo Rivero-Müller, and Arto T. Pulliainen*

Cite This: *ACS Sens.* 2020, 5, 3438–3448

Read Online

ACCESS | Metrics & More | Article Recommendations | Supporting Information

ABSTRACT: Detection of pertussis toxin (PTX) activity is instrumental for the development and manufacturing of pertussis vaccines. These quality and safety measures require thousands of mice annually. Here, we describe **I**nterference in **G**α**i**-mediated **S**ignal **T**ransduction (iGIST), an animal-free kinetic bioassay for detection of PTX, by measuring its effect on inhibitory G protein-coupled receptor (GPCR) signaling. PTX ADP-ribosylates inhibitory α-subunits of the heterotrimeric G proteins, thereby perturbing the inhibitory GPCR signaling. iGIST is based on HEK293 cells coexpressing a somatostatin receptor 2 (SSTR2), which is an inhibitory GPCR controllable by a high-affinity agonist octreotide; and a luminescent 3′5′-cyclic adenosine monophosphate (cAMP) probe. iGIST has a low sensitivity threshold in the pg/mL range of PTX, surpassing by 100-fold in a parallel analysis the currently used *in vitro* end-point technique to detect PTX, the cluster formation assay (CFA) in Chinese hamster ovary cells. iGIST also detects PTX in complex samples, i.e., a commercial PTX-toxoid-containing pertussis vaccine that was spiked with an active PTX. iGIST has an objective digital readout and is observer independent, offering prospects for automation. iGIST emerges as a promising animal-free alternative to detect PTX activity in the development and manufacturing of pertussis vaccines. iGIST is also expected to facilitate basic PTX research, including identification and characterization of novel compounds interfering with PTX.

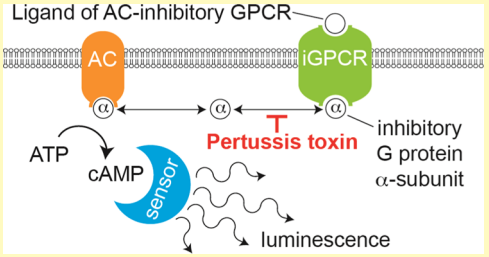

KEYWORDS: *pertussis toxin, ADP-ribosylation, G protein-coupled receptor, adenylyl cyclase, cyclic AMP, bioassay, animal-free, vaccine*

The Gram-negative bacterium *Bordetella pertussis* is the etiological agent of whooping cough, i.e., pertussis. Whooping cough is a globally distributed acute respiratory disease, affecting all age groups.[1] However, infants and young children comprise the highest-risk cohort, where the disease may lead to death despite hospital intensive care and use of antibiotics.[1] Despite the global vaccine campaign, pertussis remains endemic, causing outbreaks in many regions of the world, and the disease incidence is increasing.[2] Moreover, macrolide-resistant *B. pertussis* strains have been reported.[3,4] The data highlights the need to improve the current vaccine formulations and vaccination campaigns.

Pertussis toxin (PTX) is the major virulence factor of *B. pertussis*,[5] a protein complex secreted from the bacteria via the Sec pathway and the Ptl type IV secretion system.[6] PTX is composed of five noncovalently bound subunits (PtxS1-S5), which are arranged in an AB_5 topology.[7,8] The B_5 oligomer is formed by the PtxS2-S5 (PtxS2, PtxS3, PtxS5, and two copies of PtxS4)[7,8] and mediates binding of the secreted AB_5 holotoxin on the host cell surface in a carbohydrate-dependent manner.[8] Subsequent cell entry is followed by dissociation of the B_5 oligomer and the PtxS1.[9] The liberated PtxS1, which belongs to the family of ADP-ribosyltransferases,[10] ADP-ribosylates a single C-terminal cysteine residue in inhibitory α-subunits of most heterotrimeric ($\alpha\beta\gamma$) G protein superfamily members, such as Gαi, Gαo, and Gαt.[11−13] The resulting bulky ADP-ribose modification disrupts inhibitory α-subunit interaction with G protein-coupled receptors (GPCRs), preventing formation of the G$\alpha\beta\gamma$−GPCR complex and thereby perturbing GPCR agonist-induced signaling.[14,15] Although the pathogenic manifestations are still a matter of debate,[5] one well-recognized molecular downstream effect is altered 3′5′-cyclic adenosine monophosphate (cAMP) signaling.[16] This is attributed to the diminished inhibitory control of PTX-modified Gαi on the cAMP-producing adenylyl cyclases (ACs) (Table of Contents Graphic).

A detoxified form of PTX (PTX-toxoid) is a core component of the pertussis acellular vaccines (ACVs), where it is typically included at μg/mL levels (e.g., Boostrix lot# AC37B272AK, 16 μg/mL, used in this study). Tests for residual PTX activity are instrumental in ACV development and manufacturing. However, there are major regional differences in the regulatory guidelines.[17,18] No internationally agreed upper limit for active PTX in pertussis ACVs exists. Only China and Japan have these kinds of defined figures, of 0.8 and 0.4 histamine sensitization units/mL (HSU/mL),

Received: July 2, 2020
Accepted: October 26, 2020
Published: November 4, 2020

https://dx.doi.org/10.1021/acssensors.0c01340
ACS Sens. 2020, 5, 3438–3448

respectively, based on the mouse histamine sensitization test (HIST).[17,18] According to the WHO Annex 4 "Recommendations to assure the quality, safety and efficacy of acellular pertussis vaccines", these values correspond to 4.36 (China) and 2.18 (Japan) of international units/mL (IU/mL). In respect of the Biological Reference Preparation batch 1 (BRP1) of PTX,[19] these values are equal to 29 ng/mL (China) and 14.5 ng/mL (Japan) PTX.[17] HIST is a benchmark PTX assay in the vaccine industry capable of detecting PTX at ng/mL levels.[18] HIST is based on the early observation of PTX-treated mice becoming sensitive to histamine.[20] Mice are exposed to PTX-containing preparations, challenged with histamine, and monitored for death.[18] In the USA, for example, one undiluted single human vaccine dose of 0.5 mL is not allowed to sensitize more than 10% of the mice to histamine-induced death.[17,18] Though it has a long record in the industry, HIST is a terminal assay causing profound stress for the animals. Besides, HIST requires large amounts of animals, with recent global annual estimates of 65.000 mice.[17,18]

The most widely debated animal-free alternative to HIST builds on the early findings of Hewlett et al., who observed phenotypic alterations, described as cell rounding and cell cluster formation, in Chinese hamster ovary (CHO) cells exposed to PTX[21] (Videos S1 and S2). The resulting test, designated as a cluster formation assay (CFA), is based on visual grading of the cell clustering in CHO cell monolayers upon PTX treatment and can detect ng/mL levels of PTX.[18] However, the CFA is an observer-dependent end-point test, suffering from subjectivity bias and considerable interassay variability.[18] Also, the molecular basis of the PTX-evoked clustering in CHO cells, similar to the mechanism of histamine hypersensitivity in HIST, remains poorly understood. Despite these limitations, the European Pharmacopoeia Commission has decided that CFA can be used instead of HIST for safety assurance of the currently marketed pertussis ACVs,[18] based largely on the work of Isbrucker et al.,[22] effective as of January 2020. Recently, Biological Reference Preparation batch 1 (BRP1) of PTX was introduced to control the interassay variability of CFA.[19]

Improved alternatives to CFA, based on the mechanistic understanding of PTX cellular effects, have been actively sought for.[18] Available biochemical assays for PTX measure either the PtxS1-catalyzed ADP-ribosylation of a C-terminal peptide of Gαi with high-performance liquid chromatography (HPLC)[23] or binding of the pentameric PtxS2−S5 oligomer to carbohydrate structures with an enzyme-linked immunosorbent assay (ELISA).[24] Both the assays have objective readouts, but capture only distinct PTX activities under artificial cell-free *in vitro* conditions. DNA microarrays have been utilized to identify PTX-induced gene expression signatures either in rat tissues[25,26] or in *in vitro* cultured human cells.[27] Practical applications have not yet emerged from these studies. Hoonakker et al. exposed rat vascular smooth muscle cells (A10 cells) to PTX and determined the amount of cAMP in cell lysates with an end-point ELISA.[28] PTX did not increase the amount of cAMP when incubated alone with the cells, but it potentiated isoproterenol-induced elevation of cAMP.[28] Isoproterenol binds to β-adrenergic receptors,[29] which leads to activation of Gαs and thereby to subsequent stimulation of the cAMP-producing ACs. In an extension of their work, Hoonakker et al. detected PTX effects in A10 and CHO cells with a cAMP response element (CRE)-driven luciferase reporter.[30] In agreement with their earlier cAMP ELISA study,[28] PTX did not increase the CRE-reporter activity by itself, but it did enhance cAMP responses to isoproterenol or forskolin (FSK).[30] FSK activates ACs by intercalating the C1 and C2 subunits of ACs into the catalytically active cAMP-producing form.[31] Although the detailed molecular basis of the CRE-reporter assay was not reported, the PTX-mediated blockage of basally active Gαi signaling was probably sufficient to allow enhanced cAMP accumulation upon pharmacological AC stimulation. The CRE-reporter assay has a low ng/mL-range sensitivity for PTX,[30] comparable to CFA;[21] yet, the question of its practical use in the vaccine industry awaits further studies.

In this work,[32] we set out to establish a sensitive microtiter plate format bioassay for PTX, based on kinetic measurements of intracellular cAMP levels in living cells in combination with a defined and tightly controllable inhibitory GPCR pathway.

EXPERIMENTAL SECTION

Compounds and Reagents. All of the reagents were dissolved in ultrapure water (Milli-Q; resistivity >18 mΩ·cm), if not specified otherwise. PTX preps were obtained from List Biological Labs (#179A, Lot#179216A2A, aka $PTX_{\#1}$, stock of 200 μg/mL in 50 mM Tris, 10 mM glycine, 0.5 M NaCl, 50% (v/v) glycerol in H_2O, pH 7.5; kept aliquoted at −20 °C) and Invitrogen (#PHZ1174, Lot#75356597A, aka $PTX_{\#2}$, stock of 100 μg/mL in 10 mM Na_2HPO_4 and 50 mM NaCl in H_2O; kept aliquoted at +4 °C). Control solvents for both the PTX preps ($SolC_{\#1}$ and $SolC_{\#2}$), with a chemical composition identical to that specified above, were prepared in-house, filter-sterilized, and kept at +4 °C. Octreotide acetate was obtained from Bachem (#H-5972) and kept at −80 °C as single-use 100 μM aliquots. FSK was obtained from LC laboratories (#F-9929) and kept aliquoted (10 mM) in dimethyl sulfoxide (DMSO) at −20 °C. Boostrix vaccine was obtained from GlaxoSmithKline (tetanus toxoid, reduced diphtheria toxoid, and acellular pertussis vaccine, adsorbed, lot# AC37B272AK, 16 μg/mL formaldehyde and glutaraldehyde-inactivated PTX in 9 mg/mL NaCl with ≤0.78 mg/mL Al as aluminum hydroxide and ≤200 μg/mL Tween 80, full composition—as described by the manufacturer).

Cell Lines. Human embryonic kidney cell line (HEK293) was obtained from the American Type Culture Collection (ATCC, #CRL-1573). HEK293 with stable overexpression of the Gs22/cAMP probe, as well as the derived sensor cells with stable overexpression of SSTR2 (aka HEK-Gs/SSTR2_HA), were developed and characterized by us earlier.[33−35] Chinese hamster ovary cells (CHO) were either recovered from the local cell line repository of the Institute of Biomedicine, University of Turku, Finland (liquid N_2 storage—a cryovial of the stock culture of 1998; aka $CHO_{\#1}$), or provided as a kind gift from Dr. Aylin C. Hanyaloglu (Institute of Reproductive and Developmental Biology, Imperial College London, U.K.; aka $CHO_{\#2}$). HEK293 and CHO cells were cultured in Dulbecco's modified Eagle medium/nutrient mixture F-12 (DMEM/F-12; Gibco, #11320033), supplemented with 10% (w/v) heat-inactivated fetal bovine serum (iFBS; Biowest, #S1810), under the incubator conditions (+37 °C in humidified atmosphere with 5% CO_2). Only verified mycoplasma-negative cells were used for the experiments. Cell counts were performed using a TC20 automated cell counter (Bio-Rad Labs).

iGIST Bioassay for PTX Activity. The sensor cells were seeded on the day of the experiment into tissue culture-treated polystyrene 96-well plates with light-tight walls and a translucent bottom (ViewPlate-96, PerkinElmer, Cat#6005181) as 60 000 cells per well in 180 μL of complete medium, and incubated for 4−6 h (+37 °C in a humidified atmosphere with 5% CO_2) to allow for attachment. Next, the freshly prepared PTX dilutions or matched SolC dilutions (both in 25 mM *N*-(2-hydroxyethyl)piperazine-*N*′-ethanesulfonic acid (HEPES), pH 7.4) were added to the wells as 20 μL of 10× solutions to yield the desired 1× working concentration. Nontreated controls received 20 μL of the specified HEPES (25 mM, pH 7.4)

https://dx.doi.org/10.1021/acssensors.0c01340
ACS Sens. 2020, 5, 3438−3448

buffer per well. Further, the plates were placed back in the incubator and kept under the above-specified conditions for the scheduled time to allow for PTX to act. Once the desired exposure time had elapsed, the plates were retrieved from the incubator, the medium was removed, and the wells were refilled with 45 μL of the freshly prepared inducing medium (IndMed), comprised of 2% (v/v) GloSensor reagent (Promega, #E1290, corresponding to the final working concentration of 0.612 mg/mL, with the original stock of 30.6 mg/mL in 10 mM HEPES, pH 7.5) and a 200 μM nonselective familywide phosphodiesterase inhibitor 3-Isobutyl-1-methylxanthine (IBMX; Sigma, #I5879) in a mix of DMEM/F-12 medium (50/50, v/v) and CO_2-independent medium (Gibco, #18045-054; 4v of DMEM/F-12 per 5v of CO_2-independent medium), supplemented with 0.1% (w/v) bovine serum albumin (BSA). After equilibration for 45 min at RT in the dark, the plate was inserted into a microtiter plate reader (EnSight, PerkinElmer) and the light output, denoted as a baseline signal, was captured for 15−20 min at RT. Next, the plate was removed from the reader and the wells were spiked with either 5 μL of freshly prepared solutions, having all of the desired components at 10× of the final concentration in 25 mM HEPES, pH 7.4, or 5 μL of respective controls [i.e., HEPES solutions of either 100 nM Oct or 1% (v/v) DMSO, or just HEPES buffer]. Final concentrations of FSK and Oct in the assay equaled 10 μM and 10 nM, if not specified otherwise. As the 10 mM FSK stock was in DMSO, the final DMSO concentration in all FSK-spiked samples and DMSO controls equaled 0.1% (v/v). After spiking, the plate was immediately re-inserted into the reader and the luminescence, now denoted as induced signal, was further recorded for the time required (typically, for 45−60 min). The described assay conditions [i.e., at RT, IndMed with 2% (v/v) GloSensor reagent and 200 μM IBMX, stimulation with 10 μM FSK] are referred to as standard throughout the text. The assay with the Boostrix vaccine followed the same design. First, 20 μL of 10× of vaccine with or without external $PTX_{\#1}$ at a fixed concentration of 1000 ng/mL in Milli-Q H_2O was added to the sensor cells in 180 μL/well of the complete medium, yielding the final desired 1× of vaccine dilution (dilution range 1:10−1:10^{-6}) ± 100 ng/mL $PTX_{\#1}$. Next, the sensor cells were incubated for 24 h (+37 °C in a humidified atmosphere with 5% CO_2) before exposure to 100 nM Oct and 10 μM FSK.

For initial inspection and qualitative analyses of iGIST data, the captured luminescent reads were plotted as intracellular cAMP kinetic curves (luminescence vs time) and subjected to visual assessment. Subsequent quantitative analyses involved several steps of data transformation and were carried out as follows. First, cAMP kinetic curves were processed to obtain baseline signal-subtracted area under the curve (AUC) values by subtracting the average baseline signal from the AUC value for the period of induced signal. This was done either with the corresponding operator of GraphPad Prism software or via a custom-written script, both employing the trapezoidal rule[36] and producing similar results. The obtained AUC values were further divided by the average AUC value of FSK response in control cells (control-AUC_{FSK}), i.e., sensor cells spiked only with FSK after the baseline signal capture. This yielded FSK-normalized AUC% values (PTX-AUC% or SolC-AUC%). Finally, the PTX-AUC% and SolC-AUC% values for FSK vs FSK + Oct 10 nM responses were combined to obtain the following two ratiometric values: (i) the Gαi signal relay index [Gαi-SRI; separately calculated for PTX and SolC as AUC $\%_{FSK}/AUC\%_{FSK + Oct\ 10\ nM}$] and (ii) the comparative Gαi signal relay index [comparative Gαi-SRI; calculated as a ratio of $AUC\%_{FSK}/AUC\%_{FSK + Oct\ 10\ nM}$ for PTX to $AUC\%_{FSK}/AUC\%_{FSK + Oct\ 10\ nM}$ for SolC]. At full abrogation of Gαi signaling by PTX, the sensor cells are expected to completely lose responsiveness to Oct, with Gαi-SRI approaching 1.0. Gαi-SRI allows us to separately estimate dose effects of PTX and SolC on Gαi signaling, whilst the derived comparative Gαi-SRI integrates the effects of matched PTX and SolC doses into a single numerical value. Comparative Gαi-SRI thus accounts for any solvent effects and reveals the genuine solvent-corrected effect of PTX. Further details on luminescence data processing are covered in our earlier work.[34] A schematic of iGIST output values and of their calculations is shown in Figure S1.

CHO Cluster Formation Assay and Confluence Analysis. Cluster formation assay (CFA) was carried out based on the original descriptions by Hewlett et al.,[21] with the following modifications. CHO cells were seeded into flat-bottom 96-well plates (#655180; Greiner) as 10 000 cells/well in 180 μL of the complete medium. The plates were then placed in the incubator for 4−6 h to allow for cell attachment. Further, the cells were treated with 20 μL/well of PTX or matched SolC, as specified in the iGIST Bioassay for PTX Activity section. Next, the plates were inserted into the IncuCyte HD live cell imager (Essen BioScience), integrated with the cell culture incubator (+37 °C, humidified atmosphere with 5% CO_2), and immediately subjected to continuous phase-contrast imaging (1 snapshot every 30−60 min, up to 72 h from the moment of treatment initiation). As the culture plates were placed into the imager within 5 min of treatment, the first imaging time point was also taken as time point 0 in terms of the subsequent image analysis. No medium exchange or other perturbations were performed during the imaging.

Visual grading of morphological changes in CHO cells, exposed to different doses of PTX or matched SolC, was performed by six independent observers (two males, four females; all adults), who had never dealt with this type of analysis before. After a short introductory tutorial (a single parallel session with all of the observers) on how the grading is expected to be implemented, including review of selected examples of morphological changes in CHO cells in response to varying doses of PTX/SolC, the observers received an identical set of phase-contrast images of CHO cells, assembled as slides of 3× images each [two different fields of view (FoVs) of CHO cells in different wells of the same 96-well plate, exposed to the same dose of PTX (i.e., two technical replicates) vs one FoV of the cells that received the matched level of SolC in the same experiment]. The observers remained blinded to the PTX dose, exposure time, and CHO strain information (i.e., $CHO_{\#1}$ vs $CHO_{\#2}$), but were aware of the nature of treatments on every slide (i.e., FoVs for PTX and SolC were explicitly labeled). The grading followed a simple three-tier scale (0—no effect; 1—equivocal response; 2—clear response) and relied on visual comparison of FoV for PTX samples with the FoV of matched SolC by every observer. The resulting grades were entered into spreadsheets, available from the authors upon request, and processed to yield the average grades (out of six observers; ±SD) for every PTX dose/exposure in a given CHO strain in a given experiment. The resulting averages were eventually used to compute the respective final mean grades (with SEM and 90% CI) across several independent experiments. The final grade of 1.5 was selected for an arbitrary cutoff of a clear response. Confluence analyses for CHO cells, reflective of the surface occupancy by cells in a given FoV (with 100% corresponding to the full confluence, i.e., when an FoV is fully covered with cells), were performed using IncuCyte software (build 2010A Rev3; Confluence v.1.5 operator) on the same phase-contrast image sets that were utilized for visual grading.

Data Transformation, Curve Fitting, and Statistics. Data transformations, CI calculation, and inferential statistics were carried out using the GraphPad Prism v8.4.1 package (GraphPad Software). Dose−response curve fitting [log (inhibitor) vs response−variable slope (Y = bottom + (top − bottom)/(1 + 10^((log IC_{50} − X) × Hill slope)) for nonlinear regression and (Y = B0 + B1 × X + B2 × X^2 + B3 × X^3 + B4 × X^4 + B5 × X^5) for fifth-order polynomial regression] was performed using the respective operators of GraphPad Prism software. Comparisons of PTX vs SolC dose effects were performed using either a paired-ratio two-tailed t test or a simple two-tailed t test (for the effects, expressed as AUC%-values or through a Gαi-SRI, respectively). Level of significance was set to <0.1 for all of the tests (in the figures, one (*), two (**), three (***), and four (****) asterisks indicate p values in the following ranges: [0.05;0.1), [0.01;0.05), [0.001;0.01), and <0.001, respectively).

RESULTS AND DISCUSSION

iGIST Bioassay Robustly Detects PTX-Induced Abrogation of Gαi Signaling. iGIST is based on stably transfected HEK293 sensor cells (HEK-Gs/SSTR2_HA),

https://dx.doi.org/10.1021/acssensors.0c01340
ACS Sens. 2020, 5, 3438−3448

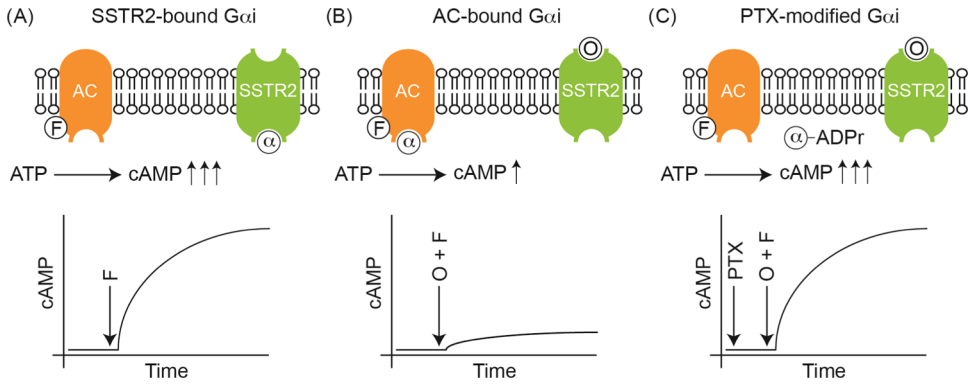

Figure 1. Schematic diagram of the molecular basis of the iGIST bioassay to detect PTX. iGIST is a living cell-based bioassay for PTX, measuring the PTX-induced alterations in G*α*i signaling in HEK293 cells, stably transfected with G*α*i-coupled SSTR2 GPCR and luminescent cAMP probe GloSensor-22F. (A) Forskolin (F) binds to and activates cAMP-producing adenylyl cyclase (AC), leading to increased generation of intracellular cAMP. (B) Octreotide (O) is a high-affinity agonist of SSTR2. Binding of octreotide to SSTR2 activates AC-inhibitory G*α*i protein (*α*), which binds to ACs and counteracts forskolin-induced generation of cAMP. (C) PTX ADP-ribosylates the AC-inhibitory G*α*i protein (*α*), thereby preventing G*α*i−SSTR2 interaction. Thus, SSTR2 cannot inhibit ACs through G*α*i any longer, and the forskolin-induced cAMP generation rate is restored.

coexpressing somatostatin receptor 2 (SSTR2), and a luminescent cAMP probe GloSensor-22F.[37,38] GloSensor-22F, originally introduced by Wood et al.,[37,38] represents a cAMP-binding domain of protein kinase A fused to a circularly permuted *Photinus pyralis* luciferase, jointly functioning as a sensitive and reversible cAMP probe in living cells. SSTR2 is used in iGIST because it can be efficiently expressed in HEK293 cells, it signals via the PTX cellular target protein G*α*i negatively regulating the cAMP-producing ACs, and its activity can be controlled by a specific ligand. The sensor cells were earlier established in-house in an HEK293 background, which has low endogenous expression of SSTR2,[34,35] and used to measure SSTR2-mediated signaling upon exposure to various ligands. In iGIST, activities of SSRT2 and ACs are controlled with a high-affinity synthetic peptide agonist octreotide (Oct)[39] and forskolin (FSK), respectively. Oct induces potent and dose-dependent activation of SSTR2 with an IC_{50} of 0.3 nM (in iGIST typically used at 10 nM).[34] FSK activates ACs by intercalating the C1 and C2 subunits into the catalytically active form,[31] which readily boosts intracellular cAMP levels and facilitates registration of counter-acting stimuli, i.e., inhibition of ACs via the Oct/SSTR2-induced G*α*i signaling. The PTX-catalyzed ADP-ribosylation of G*α*i prevents G*α*i−GPCR coupling, with ensuing loss of G*α*i-mediated inhibitory control on ACs.[11−13] A schematic of the molecular basis of iGIST bioassay is shown in Figure 1. To the best of our knowledge, no literature exists on the physiological role of SSTR2 in whooping cough. In principle, iGIST could be based on alternative inhibitory GPCRs, as long as they can be efficiently expressed and pharmacologically stimulated in sensor cells.

We incubated the sensor cells with a commercial $PTX_{\#1}$ preparation and subsequently challenged them with FSK or FSK + Oct 10 nM. Importantly, in view of the earlier noted high sensitivity of the sensor cells to certain compounds such as organic solvents and alcohols,[34] the iGIST bioassay followed a strict parallel design with every dose of $PTX_{\#1}$ evaluated against the matched dose of the $PTX_{\#1}$ solvent ($SolC_{\#1}$; 50% glycerol in H_2O with 50 mM Tris, 10 mM glycine, and 0.5 M NaCl). iGIST luminescence readout was first plotted as raw signals vs time (Figure 2A−C), which allows for quick visual assessment of the effects. Then, to obtain a quantitative observer-independent estimate of the effects, we rendered the raw luminescence signals into numerical area under the curve (AUC) values, normalized to AUC of FSK response in the control sensor cells (not exposed to $PTX_{\#1}$ or $SolC_{\#1}$ before FSK stimulation). FSK response in the control cells served as an internal calibrator in the assay and was taken as 100% for every given run. The derived values were denoted AUC% values and utilized for deduction of PTX effects on G*α*i signaling through pairwise $PTX_{\#1}$ vs $SolC_{\#1}$ comparisons (Figures 2D,E and S2). Finally, to characterize G*α*i signaling across a range of $PTX_{\#1}$ and $SolC_{\#1}$ exposures, we calculated the G*α*i signal relay index (G*α*i-SRI), expressed as a ratio of AUC% values for FSK vs combination of FSK + Oct (AUC $\%_{FSK}/AUC\%_{FSK + Oct\ 10\ nM}$; Figure 2F−H), at every given $PTX_{\#1}$ and $SolC_{\#1}$ dose. At full abrogation of G*α*i signaling by PTX, the sensor cells are expected to lose responsiveness to Oct, with G*α*i-SRI approaching 1.0. A schematic of iGIST output values and of their calculations is shown in Figure S1.

iGIST robustly registered PTX-induced abrogation of G*α*i signaling that was proportional to the $PTX_{\#1}$ dose and time in contact with the cells. iGIST demonstrated the highest sensitivity at the longest PTX incubation studied (24 h), revealing a nearly complete abrogation of G*α*i signaling even at 10 ng/mL PTX (Figures 2F and S2C,D). With shorter incubations, the PTX dose required for abrogation of G*α*i signaling increased, with the assay reliably capturing $PTX_{\#1}$ activity at 100 ng/mL with 8 h incubation (Figure 2D,E,G), and at around 1000 ng/mL with the 4 h incubation (Figures 2H and S2A,B). The global pattern of FSK response in $PTX_{\#1}$-treated sensor cells closely followed the one of $SolC_{\#1}$. Although comparisons of FSK responses at 100 ng/mL $PTX_{\#1}$ vs $SolC_{\#1}$ after 8 and 24 h reached statistical significance (Figures 2D and S2C), the actual differences were very small and thus likely had no practical relevance. The cAMP levels in the sensor cells without FSK stimulation were not significantly affected by $PTX_{\#1}$ across the dose range studied (Figure 2A−C, luminescent signals before the black arrowhead), which is in line with the earlier reports.[28,30]

As all of the above evidence was obtained with a single PTX preparation ($PTX_{\#1}$), we validated the iGIST bioassay with another PTX formulation, from a different vendor, and having a different solvent composition ($PTX_{\#2}$; in 10 mM Na_2HPO_4

https://dx.doi.org/10.1021/acssensors.0c01340
ACS Sens. 2020, 5, 3438−3448

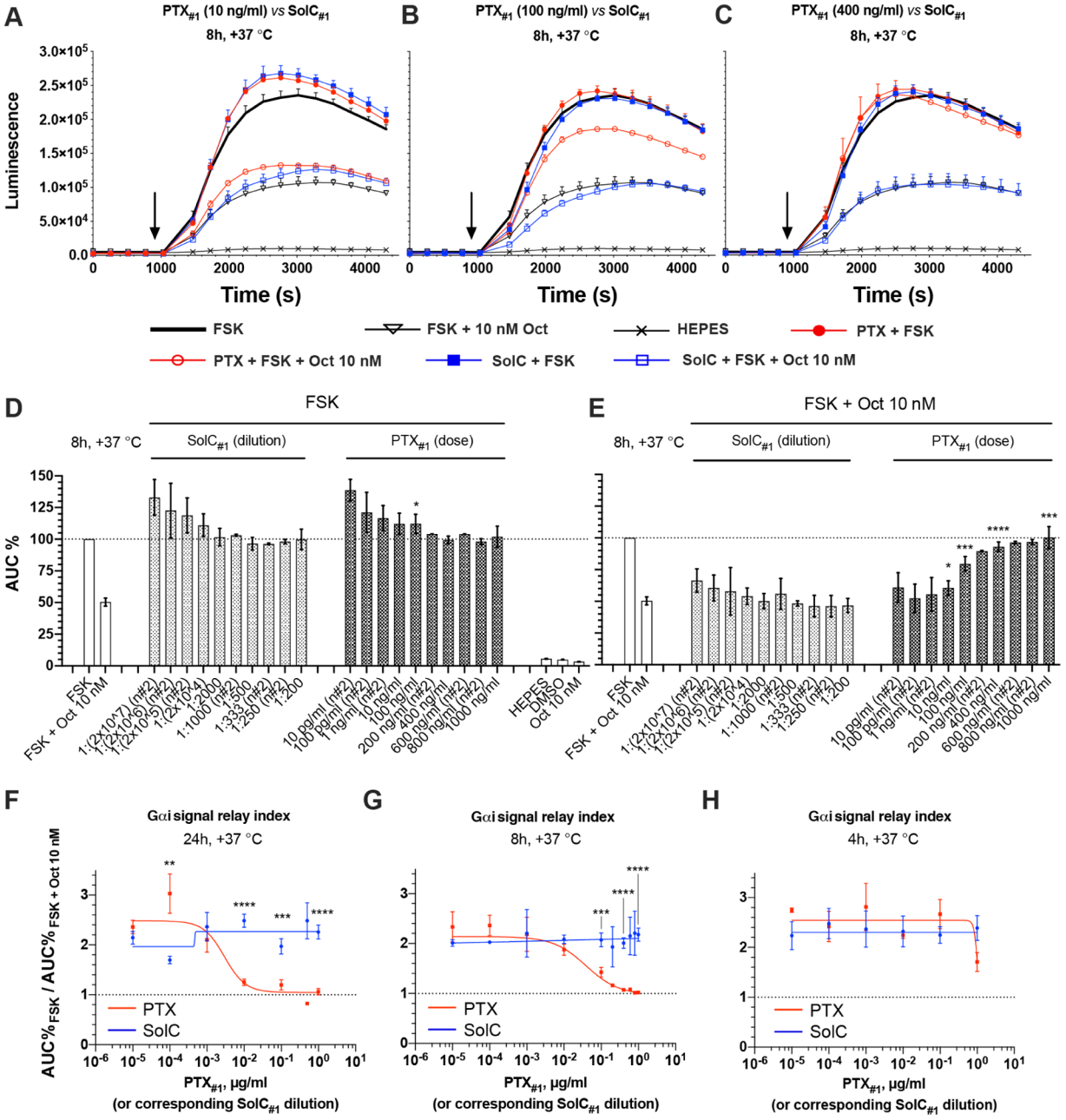

Figure 2. iGIST detects $PTX_{\#1}$-induced abrogation of Gαi signaling. (A–E) FSK and Oct responses in the sensor cells after $PTX_{\#1}$ (w/v dose) or matched $SolC_{\#1}$ (corresponding stock dilution) exposure for 8 h at +37 °C. Luminescence signals from a single representative experiment with the selected doses (A–C) and integrated results (as AUC% values) of several independent runs (D, E). For the curves in (A–C), depicting raw luminescence reads, error bars denote ±SD (only upper half shown), and *y*- and *x*-axes denote the luminescence signal (AU) and time (s), respectively. The moment of FSK and Oct addition is indicated with the black arrow. For bar diagrams in (D, E), the *y*-axis depicts AUC% values derived from the luminescence signals in several independent runs (response to FSK in control sensor cells that were not subjected to $PTX_{\#1}$ or $SolC_{\#1}$ is taken as 100%). Error bars represent average values ± SEM. (F–H) Oct/SSTR2-mediated effects on cAMP levels in sensor cells, measured as the Gαi signal relay index ($AUC\%_{FSK}/AUC\%_{FSK + Oct\ 10\ nM}$ at a given dose of $PTX_{\#1}$ or $SolC_{\#1}$) after exposure to $PTX_{\#1}$ or matched SolC for 24, 8, and 4 h at +37 °C, respectively. Panels (F, G) depict integrated results of several independent runs (average values ± SEM; see also Figure S2C,D). Panel (H) is based on data from a single representative experiment in 3× technical replicates (mean ± SD; refer also to Figure S2A,B). Dose–response curves were fitted with nonlinear regression. A state of complete abrogation of Gαi signaling ($AUC\%_{FSK}/AUC\%_{FSK + Oct\ 10\ nM} = 1$) is indicated with the black dotted line. All of the assays were run under standard conditions, in 3× technical replicates. The number of individual assay repeats (*n*#) for bar diagrams ≥3, if not indicated otherwise. Significant differences for comparisons of responses at corresponding doses of $PTX_{\#1}$ vs $SolC_{\#1}$ are indicated with asterisks (further information in the Experimental Section). Inferential statistics were measured only when $n \geq 3$ for individual assay repeats.

and 50 mM NaCl in H_2O). The response pattern of iGIST to $PTX_{\#2}$ was virtually identical to the one of $PTX_{\#1}$. Though the effect started to emerge even at 1 ng/mL $PTX_{\#2}$, abrogation of Gαi signaling became profound at 10 ng/mL toxin (Figure 3B,C)—the same threshold dose as with $PTX_{\#1}$ after 24 h incubation. Apart from a borderline increase at 10 pg/mL, $PTX_{\#2}$ did not alter the pattern of FSK response, recapitulating the effects of $SolC_{\#2}$ (Figure 3A). Basal cAMP levels before

https://dx.doi.org/10.1021/acssensors.0c01340
ACS Sens. 2020, 5, 3438–3448

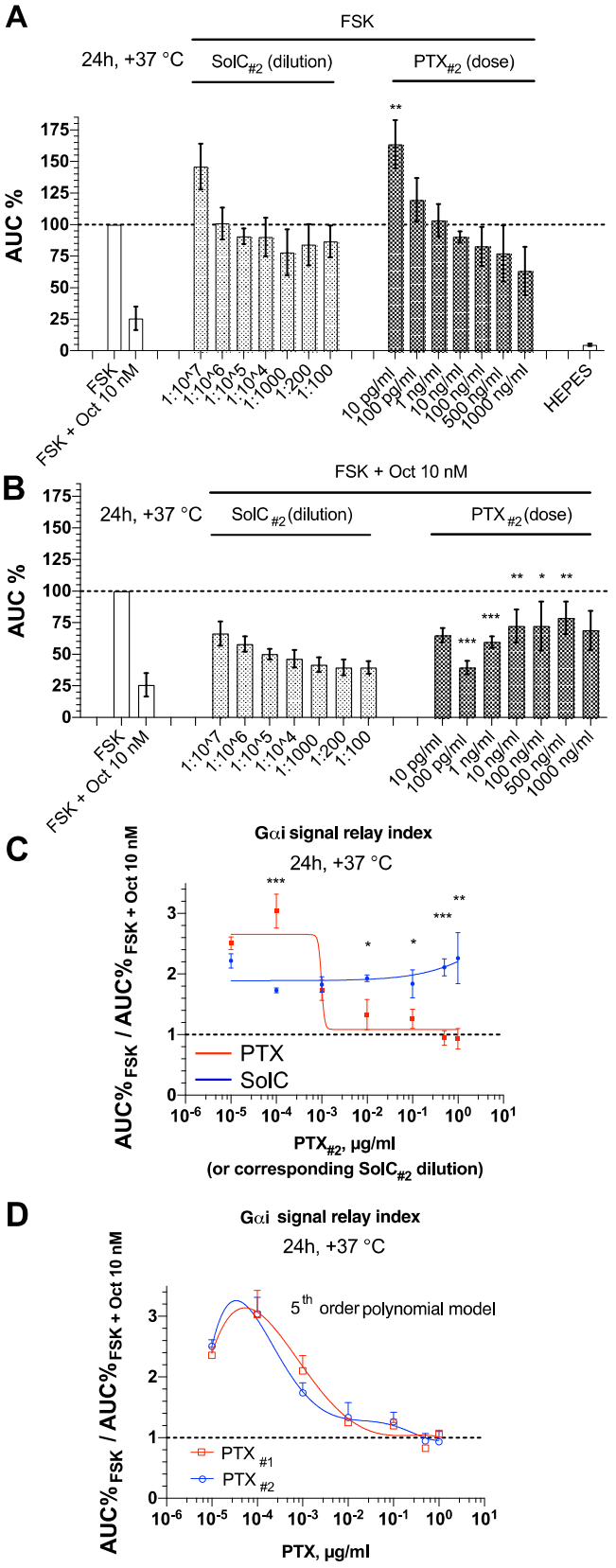

Figure 3. iGIST bioassay with $PTX_{\#2}$ and the biphasic model of PTX response. $PTX_{\#2}$ is a commercial PTX preparation from a different vendor and having a different solvent composition as compared to $PTX_{\#1}$. (A, B) FSK and Oct responses in the sensor cells after $PTX_{\#2}$ or $SolC_{\#2}$ exposure for 24 h at +37 °C; integrated results of several independent runs (number of individual assay repeats ≥3, with each assay in 3× technical replicates; shown are average values ± SEM). The *y*-axis depicts AUC% values derived from the luminescence signals (response to FSK in control sensor cells that were not subjected to $PTX_{\#2}$ or $SolC_{\#2}$ is taken as 100%). All of the assays were run under standard conditions. Significant differences for comparisons of responses at corresponding doses of $PTX_{\#2}$ vs $SolC_{\#2}$ are indicated with asterisks (further information in the Experimental Section). (C) Oct/SSTR2-mediated effects on cAMP levels in the sensor cells, measured through the Gαi signal relay index (i.e., ratio of $AUC\%_{FSK}$ and $AUC\%_{FSK + Oct\ 10\ nM}$) after exposure to $PTX_{\#2}$ (w/v dose) or matched SolC (corresponding stock dilution) for 24 at +37 °C. Curves are based on the same data as those shown in panels (A, B) (average values ± SEM), and fitted through nonlinear regression (four-parameter logistic curve with a variable slope). The state of complete abrogation of Gαi signaling ($AUC\%_{FSK}/AUC\%_{FSK + Oct\ 10\ nM}$ ratio of 1.0) is depicted with the black dotted line. (D) Gαi signal relay index ($AUC\%_{FSK}/AUC\%_{FSK + Oct\ 10\ nM}$) at different toxin doses, from $PTX_{\#1}$ and $PTX_{\#2}$ experiments with iGIST (same data points as in Figures 2F and 3C); curve fitting through a fifth-order polynomial regression.

FSK addition also stayed unaffected with $PTX_{\#2}$. Collectively, iGIST reliably detected PTX activity with two unrelated PTX preparations, revealing PTX-induced abrogation of Gαi signaling at ng/mL levels of the toxin.

iGIST Reveals an Unexpected Potentiation of Gαi Signaling at Low PTX Dose. When comparing PTX dose responses after 24 h, we unexpectedly detected potentiation of Gαi signaling with 100 pg/mL PTX, manifested as an increment of Gαi-SRI (Figures 2F and 3C). This effect seems paradoxical and difficult to understand from the standpoint of the canonical PTX activity, i.e., abrogation of Gαi signaling. Yet, the potentiation of Gαi signaling at the 100 pg/mL PTX dose was highly reproducible, pronounced, and consistently detected with both the toxin preparations ($PTX_{\#1}$ and $PTX_{\#2}$). Our initial model of PTX effect, based on Gαi-SRI and fitted through nonlinear regression (four-parameter logistic curve for an inhibitory response with a variable slope), could not accommodate this outlier. The resulting sigmoid curves (the red ones, Figures 2F and 3C) predicted a simple unidirectional inhibitory response from low ng/mL levels of PTX onward. The data prompted us to consider an alternative model of the PTX effect, which could be described by a bell-shaped curve with a truncated left arm when fitted through a fifth-order polynomial regression (Figure 3D). The resulting alternative model of PTX effects on Gαi signaling fits the experimental data much better. According to the alternative model, PTX exerts no effects on Gαi signaling at the lowest exposure tested (10 pg/mL), potentiates at 100 pg/mL dose, and starts to abrogate at higher doses. Canonical abrogation of Gαi signaling with PTX is manifested first by a decrease in Gαi-SRI back to the baseline level at around 1 ng/mL toxin (Figure 3D). This roughly corresponds to Gαi-SRI of 2—the value reflective of Gαi signaling across the studied dose range of SolCs. Then, the effect continues to increase dose dependently, reaching saturation with a nearly complete abrogation of Gαi signaling at 10 ng/mL PTX (Gαi-SRI of 1) (Figure 3D).

The potentiation of Gαi signaling by low-dose PTX in 24 h incubation, as revealed by the iGIST, is highly intriguing. Admittedly, the exact molecular basis remains a subject that requires subsequent studies. As for now, we hypothesize that

https://dx.doi.org/10.1021/acssensors.0c01340
ACS Sens. 2020, 5, 3438−3448

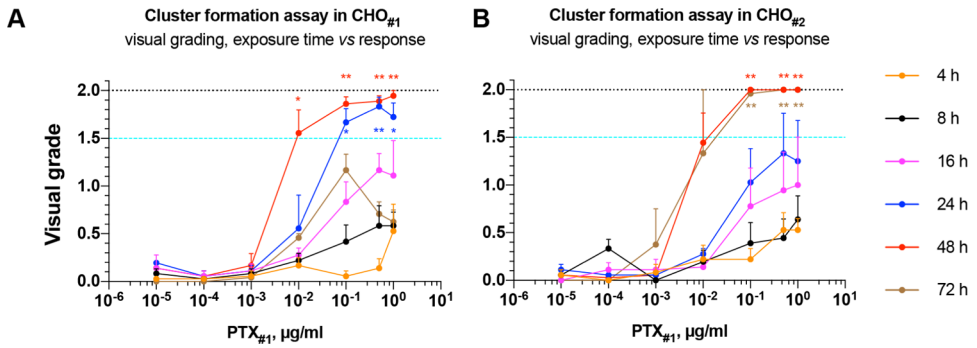

Figure 4. Cluster formation assay—visual grading of $PTX_{\#1}$-induced morphological changes in CHO cells. (A, B) $PTX_{\#1}$ dose vs incubation time studies in two strains of CHO cells ($CHO_{\#1}$ and $CHO_{\#2}$), obtained from two different sources. CHO cells were seeded into 96-well plates, treated with the indicated doses of $PTX_{\#1}$, and continuously imaged with IncuCyte HD under regular incubator conditions up to 72 h. The resulting phase-contrast images were visually graded by independent observers. The *y*-axis depicts the visual grade of morphological response in CHO (AU; average ± SEM, with only the upper half of SEM shown). The *x*-axis indicates the PTX dose. The maximal possible grade (2.0) and the preselected cutoff for a clear response (1.5) are indicated with black dotted and turquoise dashed lines, respectively. PTX exposures with a lower limit of 90% CI ≥ 1.0 or 1.5 for an average visual grade are marked with a single asterisk or double asterisks, respectively. The curve of 72 h is based on 2× independent experiments. All of the other exposure times represent combined results of 3× independent experiments (each in at least 2× technical replicates). Refer also to Figure S3.

the phenomenon relates to the dynamics of how the different G protein α-subunits are complexed and functionally regulated with G protein $\beta\gamma$-subunits.[40] However, in view of the time scale of the potentiation effect, more complex compensatory mechanisms could be involved such as a transcriptional and/or translational response. Irrespective of the nature of the underlying molecular mechanisms, detection of the potentiation effect has a profound application potential. First, it increases the sensitivity of iGIST by two orders of magnitude, from ca 10 ng/mL down to 100 pg/mL PTX. Second, it adds to the specificity of iGIST as reconstruction of the truncated bell-shaped PTX response curve through serial dilution of an analyte would ensure the specific nature of the observed signal (Figure 3D). Collectively, iGIST reveals a hitherto undescribed potentiation effect of PTX on Gαi signaling, which improves specificity and increases the sensitivity of the iGIST to pg/mL range of PTX.

iGIST Bioassay is More Sensitive than the CHO Cluster Formation Assay in Detecting PTX. The sensitivity of the iGIST bioassay was compared with that of the cluster formation assay (CFA), originally introduced by Hewlett et al..[21] To allow for direct comparison with the iGIST bioassay, we obtained two strains of wild-type CHO cells from two different sources (designated $CHO_{\#1}$ and $CHO_{\#2}$), and utilized the cells for time- and dose-range studies with the earlier used toxin preparation ($PTX_{\#1}$). Through parallel use of the two CHO strains, representing the progeny of the same maternal CHO culture, we strived to mitigate the risks, associated with possible genetic and phenotypic drift, in immortalized cell lines upon extended culturing.[41,42]

Both strains of CHO were subjected to live cell imaging with an IncuCyte HD imager under regular incubator conditions up to 72 h from the moment of PTX addition. The derived phase-contrast images were visually graded by six independent observers, using a three-tier scale (0—no effect; 1—ambiguous response; 2—clear response; all comparisons vs matched SolC) (Figures 4 and S3). With an arbitrary cutoff for a clear response set to 1.5, $CHO_{\#1}$ and $CHO_{\#2}$ demonstrated consistent and broadly similar performance in CFA. The lowest $PTX_{\#1}$ dose provoking a distinct phenotypic shift in both CHO strains was 10 ng/mL at 48 h. The perceived magnitude of phenotypic response increased further with the $PTX_{\#1}$ dose, and both $CHO_{\#1}$ and $CHO_{\#2}$ generally served as reliable PTX sensors at PTX doses of ≥100 ng/mL. However, the exposure time required for $PTX_{\#1}$-induced morphological changes to emerge did differ between the CHO strains. $CHO_{\#2}$ exhibited pronounced phenotypic alteration only after 48−72 h of exposure, whilst $CHO_{\#1}$ underwent phenotypic switch earlier, already at 24 h, with morphological alterations becoming even more pronounced at 48 h. Shorter $PTX_{\#1}$ exposure times, i.e., 16 h or less, were insufficient for induction of clear phenotypic changes in either of the CHO strains even at the highest $PTX_{\#1}$ dose tested (500−1000 ng/mL).

If we compare only absolutely clear phenotypic responses to $PTX_{\#1}$, our CFA exhibits very close performance to the CFA in the original work of Hewlett et al.[21] Also, in view of the reportedly high variation in CFA results, even with the same PTX preparations across different laboratories,[22,43,44] the described results signify the robustness of our CFA. Interestingly, automatic confluence analysis (IncuCyte software) of the same image set demonstrated a slightly improved resolution of $PTX_{\#1}$-induced effects in CHO as compared to the visual grading by the human observers (Figure S4). Here, a minor decline in estimated confluence was already noticeable at 1 ng/mL $PTX_{\#1}$ at 48 h of treatment, with the effect becoming clear and pronounced from 10 ng/mL $PTX_{\#1}$ onward. The data underlines the subjective nature of visual grading in the conventional CFA, suggesting that observer-independent software-driven image analysis might be a better option for CFA. Most importantly, however, the data demonstrates that the iGIST bioassay is more sensitive to detect $PTX_{\#1}$ than CFA (ca 100-fold, with a threshold of 100 pg/mL PTX) (Figures 2F and S2C,D).

iGIST Bioassay Detects PTX Spiked into the Boostrix Pertussis Acellular Vaccine. The commonly acknowledged limitation of CFA[21] and other proposed animal-free bioassays in detecting PTX[28,30] is their poor compatibility with the final vaccine product due to cytotoxicity of the aluminum-based adjuvants.[18] This problem still remains, despite the fact that several approaches to mitigate adjuvant toxicity, e.g., by means of vaccine dilution or barrier methods such as semipermeable transwell inserts for culture plates, have been proposed.[18] To

https://dx.doi.org/10.1021/acssensors.0c01340
ACS Sens. 2020, 5, 3438−3448

analyze the applicability of iGIST for PTX detection in complex samples, i.e., commercial pertussis vaccines, we prepared ACV dilution series supplemented with a fixed PTX concentration. As industry-grade PTX toxoid was not available, we spiked a known dose of the active $PTX_{\#1}$ to achieve a final concentration of 100 ng/mL into serial dilutions of the PTX-toxoid-containing vaccine (Boostrix, which includes 16 μg/mL PTX-toxoid, admixed with tetanus and diphtheria toxoids). Despite the complexity of Boostrix, including significant levels of aluminum (≤0.08% w/v), detergent (Tween 80), and two other toxoids (diphtheria and tetanus) with possible residual activity, iGIST successfully detected the spiked $PTX_{\#1}$. This was evidenced by the complete abrogation of Gαi signaling with Gαi-SRI of 1 in all of the analyzed Boostrix dilutions (≥1:10) (Figure 5). The unspiked Boostrix was not neutral in terms of its effects on Gαi signaling in iGIST (Figure 5C, blue dots), but in the absence of the matched SolC, the nature of the observed responses remains unknown. Importantly, we did not observe overt cytotoxicity (i.e., cell detachment, cell death) even at the most concentrated Boostrix solution tested (1:10 dilution) within the time window of the assay (24 h) (Figure S5). Taken together, our results with the $PTX_{\#1}$-spiked Boostrix underline the functional robustness of iGIST and highlight iGIST as a promising tool for PTX detection in complex samples.

iGIST-Objective Digital Readout and Prospects for Automation. An important advantage of iGIST is its observer independence. This feature, combined with the microtiter plate format and the digital nature of iGIST readout, opens avenues for automatization, e.g., by means of robotic platforms for plate handling and luminescence acquisition. Data processing at a higher throughput might be approached through utilization of tailored scripts, rendering iGIST luminescence signals into numerical values, such as Gαi-SRI ($AUC\%_{FSK}/AUC\%_{FSK + Oct\ 10\ nM}$). For an alternative numerical index of PTX activity that streamlines data interpretation and thus might be more compatible with automated data processing, we propose a comparative Gαi-SRI, calculated as a ratio of ($AUC\%_{FSK}/AUC\%_{FSK + Oct\ 10\ nM}$) values for PTX-exposed and matched SolC-exposed samples (Figure S6). Reflective of the relative change in Gαi signaling in the sensor cells, be it potentiation or abrogation, and accounting for the effects of SolC, comparative Gαi-SRI should readily highlight PTX exposures. Comparative Gαi-SRI can also be used to measure iGIST interassay variability, i.e., we obtained a three-point composite estimate of 15.23% (equaling average coefficient of variation for comparative Gαi-SRIs for PTX 10 pg/mL, 100 pg/mL, and 10 ng/mL at 24 h of exposure, taken as no-effect level, maximal stimulation, and inhibition, respectively, for 4× independent runs). Subsequent studies with appropriate controls, i.e., individual vaccine components and SolCs from different steps of the PTX vaccine manufacturing process, are required to delineate the industry-scale applicability of iGIST.

CONCLUSIONS

We established **I**nterference in **Gαi**-mediated **S**ignal **T**ransduction (iGIST), a kinetic microtiter plate format bioassay to detect PTX at pg/mL levels, by measuring its effect on inhibitory GPCR signaling. iGIST is observer independent, has an objective digital readout, and exceeds in sensitivity by 100-fold the currently used *in vitro* end-point technique to detect PTX activity, the cluster formation assay in Chinese hamster ovary cells.[18] iGIST also detects PTX in complex samples, i.e., a commercial PTX-toxoid containing pertussis vaccine Boostrix that was spiked with an active PTX. We conclude that iGIST is a useful new tool for PTX basic research,[5] PTX-targeted drug development,[45] and PTX-focused industrial applications including the development and manufacturing of PTX-toxoid containing pertussis vaccines.[18] Performed in microtiter plates,

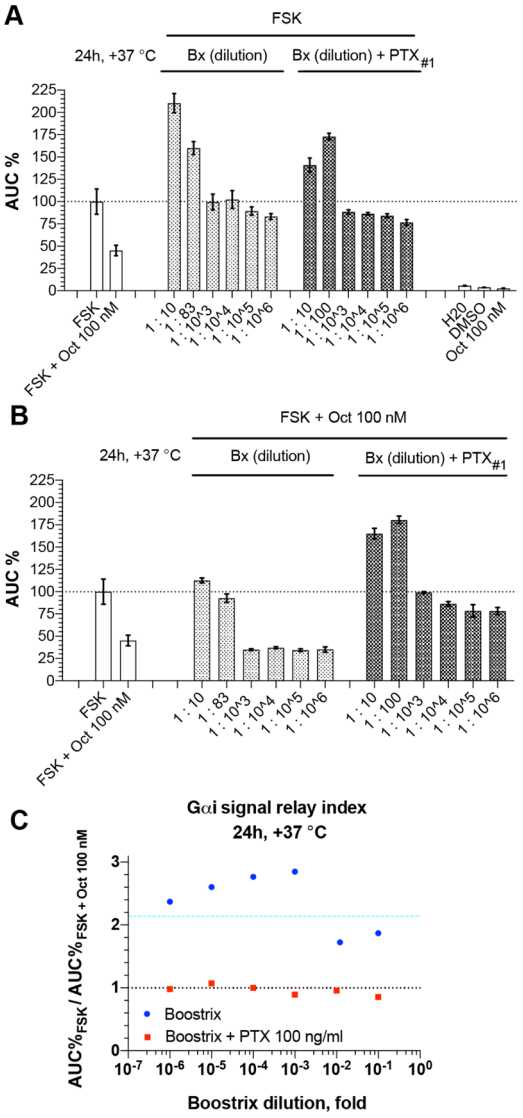

Figure 5. iGIST bioassay detects $PTX_{\#1}$ spiked into Boostrix pertussis ACV. (A, B) FSK and Oct responses in the sensor cells after 24 h/+37 °C pre-incubation with serial dilutions of either Boostrix vaccine or Boostrix vaccine admixed with a fixed dose of $PTX_{\#1}$ (final $PTX_{\#1}$ concentration—100 ng/mL). Data from a representative run in 3× technical replicates (average values ± SD), performed under standard conditions. The *y*-axis indicates AUC% values (response to FSK in control cells, which received neither Boostrix nor Boostrix with $PTX_{\#1}$, is taken as 100%), Boostrix dilution of 1:83 on panels (A, B) (vs the intended 1:100 dilution) is a result of an inadvertent pipetting mistake. (C) Gαi signal relay index ($AUC\%_{FSK}/AUC\%_{FSK + Oct\ 10\ nM}$) vs vaccine dose, based on the data in panels (A, B) (average values depicted). Gαi signaling after exposure to $SolC_{\#1}$ and the state of complete abrogation of Gαi signaling are shown with turquoise dashed (Gαi-SRI = 2.14) and black dotted (Gαi-SRI = 1.0) lines, respectively. Gαi-SRI for 100 ng/mL $PTX_{\#1}$ w/o vaccine equaled 1022 (not shown). A Higher Oct dose (100 nM) was utilized in the assay to ensure potent SSTR2 activation, thus minimizing possible effects of vaccine components on Gαi signaling.

https://dx.doi.org/10.1021/acssensors.0c01340
ACS Sens. 2020, 5, 3438−3448

iGIST has potential for automation and batch processing, both required for industrial applications. Most importantly, iGIST is an animal-free assay and thereby emerges as a promising alternative to complement or to replace mouse histamine sensitization test (HIST), the current vaccine industry standard to detect PXT activity.[18] A better understanding of practical prospects for iGIST in industrial applications would follow from future rigorous head-to-head studies (iGIST vs comparators) with reference PTX, such as Biological Reference Preparation batch 1 (BRP1), and PTX-toxoid formulations, such as industrial PTX patches before and after detoxification. Further experimentation is also warranted on the compatibility of iGIST with the final vaccine formulations, e.g., to enable studies on the important aspect of PTX activity reversal in long-term pertussis ACV storage. These studies should preferentially be performed as a multi-institutional collaborative effort to ensure standardization and transferability.

■ ASSOCIATED CONTENT

Supporting Information

The Supporting Information is available free of charge at https://pubs.acs.org/doi/10.1021/acssensors.0c01340.

Schematic representation of iGIST output values and of their calculations (Figure S1); iGIST AUC%-value results with 4 and 24 h $PTX_{\#1}$ exposures (Figure S2); phase-contrast images of $PTX_{\#1}$-induced clustering in monolayers of CHO cells (Figure S3); quantitation of $PTX_{\#1}$-induced clustering in monolayers of CHO cells by computer-aided confluence analysis (Figure S4); phase-contrast images of the sensor cells upon exposure to varying levels of Boostrix (Figure S5); and iGIST-objective digital readout and prospects for automation (Figure S6) (PDF)

Time-lapse movies of the phase-contrast images for $CHO_{\#1}$ with 100 ng/mL $PTX_{\#1}$ (Video S1) (MPG)

Time-lapse movies of the phase-contrast images for $CHO_{\#1}$ with the matched SolC control (Video S2) (MPG)

■ AUTHOR INFORMATION

Corresponding Author

Arto T. Pulliainen − *Institute of Biomedicine, Research Unit for Infection and Immunity, University of Turku, FI-20520 Turku, Finland;* orcid.org/0000-0002-9361-8963; Phone: +358-(0)40-1586044; Email: arto.pulliainen@utu.fi

Authors

Valeriy M. Paramonov − *Institute of Biomedicine, Research Unit for Integrative Physiology and Pharmacology, University of Turku, FI-20520 Turku, Finland; Turku Bioscience Centre, University of Turku and Åbo Akademi University, FI-20520 Turku, Finland; Faculty of Science and Engineering, Cell Biology, Åbo Akademi University, FI-20500 Turku, Finland*

Cecilia Sahlgren − *Turku Bioscience Centre, University of Turku and Åbo Akademi University, FI-20520 Turku, Finland; Faculty of Science and Engineering, Cell Biology, Åbo Akademi University, FI-20500 Turku, Finland; Institute for Complex Molecular Systems, Eindhoven University of Technology, 5612 AZ Eindhoven, The Netherlands*

Adolfo Rivero-Müller − *Institute of Biomedicine, Research Unit for Integrative Physiology and Pharmacology, University of Turku, FI-20520 Turku, Finland; Department of Biochemistry and Molecular Biology, Medical University of Lublin, 20-059 Lublin, Poland;* orcid.org/0000-0002-9794-802X

Complete contact information is available at: https://pubs.acs.org/10.1021/acssensors.0c01340

Author Contributions

The manuscript was written through contributions of all authors. All authors have given approval to the final version of the manuscript.

Notes

The authors declare no competing financial interest.

■ ACKNOWLEDGMENTS

The authors thank Alexander V. Travov for excellent technical assistance (writing a script for processing of luminescence data) and critical outlook. Alex-Mikael Barkoff is acknowledged for the valuable discussions on pertussis. This work was supported by European Community Mobility Programme EMA2 (Grant #372117-1-2012-1-FI-ERAMUNDUS-EMA21; to V.M.P.), the Turku Doctoral Programme of Molecular Medicine (TuDMM; to V.M.P.), K. Albin Johanssons Stiftelse (to V.M.P.), Ida Montinin Säätiö (to V.M.P.), Pentti and Tyyni Ekbom Foundation (to V.M.P.), Instrumentarium Science Foundation (to V.M.P.), Sigrid Juselius Foundation (to A.T.P.), and the Academy of Finland (Grant No. 295296; to A.T.P.).

■ ABBREVIATIONS

AC/ACs, adenylyl cyclase/s; ACV/ACVs, acellular vaccine/s; ATCC, American Type Culture Collection; AU, arbitrary units; AUC, area under curve; cAMP, 3′5′-cyclic adenosine monophosphate; BSA, bovine serum albumin; CFA, cluster formation assay; CHO, Chinese hamster ovary cells; CI, confidence interval; CRE, cAMP response element; DMEM, Dulbecco's modified Eagle medium; IndMed, inducing medium; FoV, field of view; FSK, forskolin; GPCR/GPCRs, G protein-coupled receptor/s; HIST, mouse histamine sensitization test; IC_{50}, concentration of a compound, triggering half of the maximum inhibitory effect; iGIST, interference in Gαi-mediated signal transduction, a bioassay for PTX; iFBS, heat-inactivated fetal bovine serum; ns, non-significant; Oct, octreotide; ON, overnight; PTX, pertussis toxin; RT, room temperature; SD, standard deviation; SEM, standard error of the mean; SolC, solvent control (for PTX); SRI, signal relay index; SSTR2, somatostatin receptor 2

■ REFERENCES

(1) Kilgore, P. E.; Salim, A. M.; Zervos, M. J.; Schmitt, H. J. Pertussis: microbiology, disease, treatment, and prevention. *Clin. Microbiol. Rev.* **2016**, *29*, 449−486.

(2) Skoff, T. H.; Baumbach, J.; Cieslak, P. R. Tracking pertussis and evaluating control measures through enhanced pertussis surveillance, Emerging Infections Program, United States. *Emerg. Infect. Dis.* **2015**, *21*, 1568−1573.

(3) Guillot, S.; Descours, G.; Gillet, Y.; Etienne, J.; Floret, D.; Guiso, N. Macrolide-resistant *Bordetella pertussis* infection in newborn girl, France. *Emerg. Infect. Dis.* **2012**, *18*, 966−968.

(4) Wang, Z.; Li, Y.; Hou, T.; Liu, X.; Liu, Y.; Yu, T.; Chen, Z.; Gao, Y.; Li, H.; He, Q. Appearance of macrolide-resistant *Bordetella pertussis* strains in China. *Antimicrob. Agents Chemother.* **2013**, *57*, 5193−5194.

(5) Scanlon, K.; Skerry, C.; Carbonetti, N. Association of pertussis toxin with severe pertussis disease. *Toxins* **2019**, *11*, No. 373.

(6) Weiss, A. A.; Johnson, F. D.; Burns, D. L. Molecular characterization of an operon required for pertussis toxin secretion. *Proc. Natl. Acad. Sci. U.S.A.* **1993**, *90*, 2970−2974.
(7) Stein, P. E.; Boodhoo, A.; Armstrong, G. D.; Cockle, S. A.; Klein, M. H.; Read, R. J. The crystal structure of pertussis toxin. *Structure* **1994**, *2*, 45−57.
(8) Stein, P. E.; Boodhoo, A.; Armstrong, G. D.; Heerze, L. D.; Cockle, S. A.; Klein, M. H.; Read, R. J. Structure of a pertussis toxin-sugar complex as a model for receptor binding. *Nat. Struct. Mol. Biol.* **1994**, *1*, 591−596.
(9) Hazes, B.; Boodhoo, A.; Cockle, S. A.; Read, R. J. Crystal structure of the pertussis toxin-ATP complex: a molecular sensor. *J. Mol. Biol.* **1996**, *258*, 661−671.
(10) Simon, N. C.; Aktories, K.; Barbieri, J. T. Novel bacterial ADP-ribosylating toxins: structure and function. *Nat. Rev. Microbiol.* **2014**, *12*, 599−611.
(11) Katada, T.; Ui, M. Direct modification of the membrane adenylate cyclase system by islet-activating protein due to ADP-ribosylation of a membrane protein. *Proc. Natl. Acad. Sci. U.S.A.* **1982**, *79*, 3129−3133.
(12) West, R. E., Jr.; Moss, J.; Vaughan, M.; Liu, T.; Liu, T. Y. Pertussis toxin-catalyzed ADP-ribosylation of transducin. Cysteine 347 is the ADP-ribose acceptor site. *J. Biol. Chem.* **1985**, *260*, 14428−14430.
(13) Graf, R.; Codina, J.; Birnbaumer, L. Peptide inhibitors of ADP-ribosylation by pertussis toxin are substrates with affinities comparable to those of the trimeric GTP-binding proteins. *Mol. Pharmacol.* **1992**, *42*, 760−764.
(14) Conklin, B. R.; Farfel, Z.; Lustig, K. D.; Julius, D.; Bourne, H. R. Substitution of three amino acids switches receptor specificity of Gq alpha to that of Gi alpha. *Nature* **1993**, *363*, 274−276.
(15) Draper-Joyce, C. J.; Khoshouei, M.; Thal, D. M.; Liang, Y. L.; Nguyen, A. T. N.; Furness, S. G. B.; Venugopal, H.; Baltos, J. A.; Plitzko, J. M.; Danev, R.; Baumeister, W.; May, L. T.; Wootten, D.; Sexton, P. M.; Glukhova, A.; Christopoulos, A. Structure of the adenosine-bound human adenosine A_1 receptor-Gi complex. *Nature* **2018**, *558*, 559−563.
(16) Katada, T.; Ui, M. ADP ribosylation of the specific membrane protein of C6 cells by islet-activating protein associated with modification of adenylate cyclase activity. *J. Biol. Chem.* **1982**, *257*, 7210−7216.
(17) Hoonakker, M.; Arciniega, J.; Hendriksen, C. Safety testing of acellular pertussis vaccines: Use of animals and 3Rs alternatives. *Hum. Vaccines Immunother.* **2017**, *13*, 2522−2530.
(18) Markey, K.; Asokanathan, C.; Feavers, I. Assays for determining pertussis toxin activity in acellular pertussis vaccines. *Toxins* **2019**, *11*, No. 417.
(19) Markey, K.; Douglas-Bardsley, A.; Hockley, J.; Le Tallec, D.; Costanzo, A. Calibration of pertussis toxin BRP batch 1 in a standardised CHO cell-based clustering assay. *Pharmeur. Bio Sci. Notes* **2018**, *2018*, 112−123.
(20) Parfentjev, I. A.; Goodline, M. A. Histamine shock in mice sensitized with *Hemophilus pertussis* vaccine. *J. Pharmacol. Exp. Ther.* **1948**, *92*, 411−413.
(21) Hewlett, E. L.; Sauer, K. T.; Myers, G. A.; Cowell, J. L.; Guerrant, R. L. Induction of a novel morphological response in Chinese hamster ovary cells by pertussis toxin. *Infect. Immun.* **1983**, *40*, 1198−1203.
(22) Isbrucker, R.; Daas, A.; Wagner, L.; Costanzo, A. Transferability study of CHO cell clustering assays for monitoring of pertussis toxin activity in acellular pertussis vaccines. *Pharmeur. Bio Sci. Notes* **2016**, *2015*, 97−114.
(23) Cyr, T.; Menzies, A. J.; Calver, J.; Whitehouse, L. W. A quantitative analysis for the ADP-ribosylation activity of pertussis toxin: an enzymatic-HPLC coupled assay applicable to formulated whole cell and acellular pertussis vaccine products. *Biologicals* **2001**, *29*, 81−95.
(24) Gomez, S. R.; Xing, D. K.; Corbel, M. J.; Coote, J.; Parton, R.; Yuen, C. T. Development of a carbohydrate binding assay for the B-oligomer of pertussis toxin and toxoid. *Anal. Biochem.* **2006**, *356*, 244−253.
(25) Hamaguchi, I.; Imai, J.; Momose, H.; Kawamura, M.; Mizukami, T.; Naito, S.; Maeyama, J.; Masumi, A.; Kuramitsu, M.; Takizawa, K.; Kato, H.; Mizutani, T.; Horiuchi, Y.; Nomura, N.; Watanabe, S.; Yamaguchi, K. Application of quantitative gene expression analysis for pertussis vaccine safety control. *Vaccine* **2008**, *26*, 4686−4696.
(26) Momose, H.; Mizukami, T.; Ochiai, M.; Hamaguchi, I.; Yamaguchi, K. A new method for the evaluation of vaccine safety based on comprehensive gene expression analysis. *J. Biomed. Biotechnol.* **2010**, *2010*, No. 361841.
(27) Vaessen, S. F.; Bruysters, M. W.; Vandebriel, R. J.; Verkoeijen, S.; Bos, R.; Krul, C. A.; Akkermans, A. M. Toward a mechanism-based in vitro safety test for pertussis toxin. *Hum. Vaccines Immunother.* **2014**, *10*, 1391−1395.
(28) Hoonakker, M. E.; Ruiterkamp, N.; Hendriksen, C. F. The cAMP assay: a functional in vitro alternative to the in vivo Histamine Sensitization test. *Vaccine* **2010**, *28*, 1347−1352.
(29) Warne, T.; Moukhametzianov, R.; Baker, J. G.; Nehmé, R.; Edwards, P. C.; Leslie, A. G.; Schertler, G. F.; Tate, C. G. The structural basis for agonist and partial agonist action on a $\beta(1)$-adrenergic receptor. *Nature* **2011**, *469*, 241−244.
(30) Hoonakker, M. E.; Verhagen, L. M.; van der Maas, L.; Sloots, A.; Hendriksen, C. F. M. Reporter cell lines for detection of pertussis toxin in acellular pertussis vaccines as a functional animal-free alternative to the in vivo histamine sensitization test. *Vaccine* **2017**, *35*, 1152−1160.
(31) Tesmer, J. J.; Sunahara, R. K.; Gilman, A. G.; Sprang, S. R. Crystal structure of the catalytic domains of adenylyl cyclase in a complex with Gsalpha.GTPgammaS. *Science* **1997**, *278*, 1907−1916.
(32) Paramonov, V. M.; Sahlgren, C.; Rivero-Müller, A.; Pulliainen, A. T. iGIST - a kinetic bioassay for pertussis toxin based on its effect on inhibitory GPCR signaling *bioRxiv* **2020**, DOI: 10.1101/2020.09.29.318451.
(33) Trehan, A.; Rotgers, E.; Coffey, E. T.; Huhtaniemi, I.; Rivero-Müller, A. CANDLES, an assay for monitoring GPCR induced cAMP generation in cell cultures. *Cell Commun. Signal.* **2014**, *12*, No. 70.
(34) Paramonov, V. M.; Desai, D.; Kettiger, H.; Mamaeva, V.; Rosenholm, J. M.; Sahlgren, C.; Rivero-Müller, A. Targeting somatostatin receptors by functionalized mesoporous silica nanoparticles - are we striking home? *Nanotheranostics* **2018**, *2*, 320−346.
(35) Paramonov, V. M.; Mamaeva, V.; Sahlgren, C.; Rivero-Müller, A. Genetically-encoded tools for cAMP probing and modulation in living systems. *Front. Pharmacol.* **2015**, *6*, No. 196.
(36) Burden, R. L.; Faires, D. J.; Burden, A. M. *Numerical Analysis*, 10th ed.; Brooks Cole, 2015.
(37) Binkowski, B. F.; Butler, B. L.; Stecha, P. F.; Eggers, C. T.; Otto, P.; Zimmerman, K.; Vidugiris, G.; Wood, M. G.; Encell, L. P.; Fan, F.; Wood, K. V. A luminescent biosensor with increased dynamic range for intracellular cAMP. *ACS Chem. Biol.* **2011**, *6*, 1193−1197.
(38) Fan, F.; Binkowski, B. F.; Butler, B. L.; Stecha, P. F.; Lewis, M. K.; Wood, K. V. Novel genetically encoded biosensors using firefly luciferase. *ACS Chem. Biol.* **2008**, *3*, 346−351.
(39) Bauer, W.; Briner, U.; Doepfner, W.; Haller, R.; Huguenin, R.; Marbach, P.; Petcher, T. J.; Pless, J. SMS 201-995: a very potent and selective octapeptide analogue of somatostatin with prolonged action. *Life Sci.* **1982**, *31*, 1133−1140.
(40) Hillenbrand, M.; Schori, C.; Schöppe, J.; Plückthun, A. Comprehensive analysis of heterotrimeric G-protein complex diversity and their interactions with GPCRs in solution. *Proc. Natl. Acad. Sci. U.S.A.* **2015**, *112*, E1181−E1190.
(41) Hughes, P.; Marshall, D.; Reid, Y.; Parkes, H.; Gelber, C. The costs of using unauthenticated, over-passaged cell lines: how much more data do we need? *Biotechniques* **2007**, *43*, 575.
(42) Liu, Y.; Mi, Y.; Mueller, T.; Kreibich, S.; Williams, E. G.; Van Drogen, A.; Borel, C.; Frank, M.; Germain, P. L.; Bludau, I.; Mehnert, M.; Seifert, M.; Emmenlauer, M.; Sorg, I.; Bezrukov, F.; Bena, F. S.; Zhou, H.; Dehio, C.; Testa, G.; Saez-Rodriguez, J.; Antonarakis, S. E.;

Hardt, W. D.; Aebersold, R. Multi-omic measurements of heterogeneity in HeLa cells across laboratories. *Nat. Biotechnol.* **2019**, *37*, 314−322.
(43) Douglas-Bardsley, A.; Asokanathan, C.; Tierney, S.; Hockley, J.; Markey, K. Collaborative study for the calibration of the replacement International Standard for pertussis toxin for use in histamine sensitisation and CHO cell clustering assays. *Biologicals* **2019**, *62*, 85−92.
(44) Xing, D.; Das, R. G.; Newland, P.; Corbel, M. Comparison of the bioactivity of reference preparations for assaying *Bordetella pertussis* toxin activity in vaccines by the histamine sensitisation and Chinese hamster ovary-cell tests: assessment of validity of expression of activity in terms of protein concentration. *Vaccine* **2002**, *20*, 3535−3542.
(45) Ashok, Y.; Miettinen, M.; Oliveira, D. K. H.; Tamirat, M. Z.; Näreoja, K.; Tiwari, A.; Hottiger, M. O.; Johnson, M. S.; Lehtiö, L.; Pulliainen, A. T. Discovery of Compounds Inhibiting the ADP-Ribosyltransferase Activity of Pertussis Toxin. *ACS Infect. Dis.* **2020**, *6*, 588−602.

https://dx.doi.org/10.1021/acssensors.0c01340
ACS Sens. 2020, 5, 3438−3448